Probing and extracting the structure of vibrating SF₆ molecules with inner-shell photoelectrons

Ngoc-Ty Nguyen,[1,2] R. R. Lucchese,[3] C. D. Lin,[1] and Anh-Thu Le[1]

[1]*Department of Physics, Cardwell Hall, Kansas State University, Manhattan, Kansas 66506, USA*

[2]*Department of Physics, University of Pedagogy, 280 An Duong Vuong, Ward 5, Ho Chi Minh City, Vietnam*

[3]*Department of Chemistry, Texas A&M University, College Station, Texas 77843-3255, USA*

We propose a scheme for probing the structure of vibrating molecules with photoelectrons generated from ultrashort soft-x-ray pulses. As an example we analyze below-100-eV photoelectrons liberated from the $S(2p)$ orbital of vibrating SF₆ molecules to image very small structural changes of molecular vibration. In particular, photoionization cross sections and photoelectron angular distributions (PAD) at nonequilibrium geometries can be retrieved accurately with photoelectrons near the shape resonance at 13 eV. This is achieved with a pump-probe scheme, in which the symmetric stretch mode is first Raman excited predominantly by a relatively short laser pulse and then later probed at different time delays by a few-femtosecond soft-x-ray pulse with photon energy near 200 eV.

I. INTRODUCTION

Imaging the internal molecular structures has always been one of grand challenges in physics, chemistry, and biology. Most of our knowledge on molecular structure has so far been derived from x-ray and electron diffraction measurements. With the advent of ultrashort intense lasers [1] and x-ray free electron lasers (XFELs) [2–5], ultrafast imaging with femtosecond temporal resolution and sub-Ångström spatial resolution is becoming a very active research area with the promise of providing a "molecular movie" of the dynamics of a chemical process. Apart from the more traditional approaches based on x-ray diffraction [2,6] and ultrafast electron diffraction (UED) [7], methods based on the recollision phenomena with intense driving lasers have been proposed and successfully tested on simple molecules. We mention here high-order harmonic-generation (HHG) spectroscopy [8–12] and laser-induced electron diffraction (LIED) [9,13–18]. Time-resolved photoelectron spectroscopy (TRPES) and time-resolved molecular-frame photoelectron angular distribution (TRMFPAD) measurements proposed recently [19,20] are capable of imaging valence-electron dynamics and atom motion during a chemical reaction. In this approach, the temporal resolution is limited to about hundreds of femtoseconds, owing mostly to the vacuum ultraviolet (VUV) laser pulse duration used in the experiments.

Since x-ray diffraction suffers from weak elastic scattering cross sections, to take advantage of the currently available and future short extreme ultraviolet (XUV) or x-ray pulses, different schemes have been proposed for gas-phase molecules which rely on photoelectron diffraction [21–29]. In contrast to the TRPES method that probes valence electrons, photoelectron diffraction with localized inner-shell electrons is capable of directly imaging atomic positions. In Ref. [23], multiple scattering theory was used to fit to experimental photoelectron diffraction images to extract bond lengths and bond angles for small oriented molecules. It has been shown that the method can be extended to laser-aligned molecules [30,31]. In Ref. [32], C–C bond length was retrieved from experimental "double-slit" interference pattern by photoelectrons resulting from ionizing inner shell $C(2s)$ in simple hydrocarbons. So far, most of these works have been limited to static targets.

In this paper we propose a scheme of applying short (subfemtosecond to few-femtosecond) soft-x-ray pulses for inner-shell photoelectron spectroscopy to follow fast dynamics of the nuclear wave packet and to extract photoionization cross sections for molecules away from equilibrium geometries. Although imaging with photoelectron diffraction works in principle with a broad range of energy, we choose to illustrate the method near a shape resonance, where the photoelectron signal is significantly enhanced. As is well known, shape resonances in photoionization (or photoabsorption) are caused by temporary trapping of the photoelectron by a dynamical angular-momentum barrier [33] during its emission. Usually it can also be thought of as an electron making a transition to an unoccupied valence molecular orbital embedded in the continuum that later decays to release the photoelectron. Shape resonances are thus expected to be very sensitive to atomic positions in molecules.

To be specific, we demonstrate the method by probing small-amplitude vibrations in SF₆ in real time. SF₆ was chosen because it is known to have very pronounced shape resonances for transition from $S(2p)$ to $2t_{2g}$ and $4e_g$ at photon energy near 185 and 195 eV, respectively [34,35]—the ionization energy from $S(2p)$ is 180.67 eV [36]. Similar shape resonances exist for valence electrons, but they are significantly less pronounced [37,38]. The schematic of energy levels of relevant molecular orbitals (MO) is shown in Fig. 1(a).

Briefly, the present method is based on the Raman pump–soft-x-ray-probe scheme, illustrated schematically in Fig. 1(b). An SF₆ molecule is first Raman excited predominantly to the symmetric stretch mode by a relatively weak and short infrared laser pulse. Its nuclear dynamics is later probed at different time delays by a short (subfemtosecond to few-femtosecond) soft-x-ray pulse. By analyzing photoelectron signals from $S(2p)$ for fixed photoelectron energies as a function of time delay, we extract time-dependent nuclear wave packet and photoionization cross sections at positions away from the equilibrium geometry. The photon energy is carefully chosen to be near 200 eV, such that photoelectron from $S(2p)$ have relatively small kinetic energies and well-separated energetically from other channels. During its emission, a low-energy photoelectron spends longer time in the vicinity
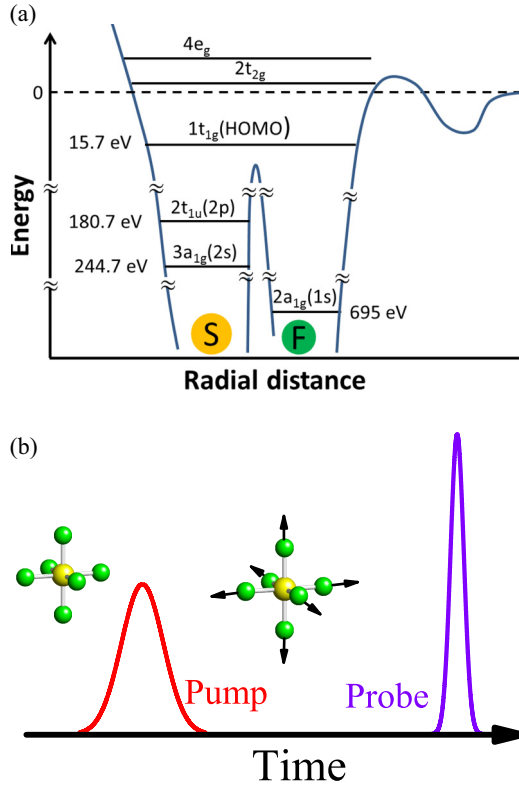
FIG. 1. (a) Schematic of relevant molecular orbitals (MOs) of SF_6 and the potential barrier. Experimental ionization potentials are taken from Refs. [36] and [37]. (b) Schematic of Raman-pump–soft-x-ray-probe experiment.

of the surrounding atoms and thus is more influenced by their precise positions. Although the technique should be applicable for a wide range of photoelectron energy, we show that it is most efficient for the photoelectrons near the $4e_g$ shape resonance at 13 eV, where the photoionization cross section is most sensitive to the nuclear geometry. Since $S(2p)$ orbital (or more precisely, $2t_{1u}$) is nearly unchanged during the vibration, these photoelectrons, in essence, probe the changes in the resonance state $4e_g$ in real time.

The rest of this paper is organized as follows: In Sec. II, we briefly describe the theoretical method, namely, the simulation of vibrational Raman excitation and calculation of photoionization cross section (PICS) and photoelectron angular distribution (PAD). The main results are presented in Sec. III, where we analyze the behavior of the photoelectron signal vs pump-probe delay time. The theoretical predictions demonstrate qualitative differences in the spectra that can be tested with future experiments. The differences encode information of photoionization cross sections as a function of the S-F bond length. We further show how the photoionization cross section and nuclear wave packets can be retrieved from those data. Finally, we finish our paper with a summary and outlook in Sec. IV.

II. THEORETICAL METHOD

A. Vibrational Raman excitation

Raman excitation of SF_6 by short Ti:sapphire laser pulses (with wavelength near 800 nm) has been studied before (see,

for example, Refs. [39,40]). It was shown [39] that, with a typical laser intensity of 5×10^{13} W/cm^2 and pulse duration of 30 fs, the symmetric stretch mode (A_{1g} at 775 cm^{-1}, to be denoted in the following also as v_1) is dominantly populated while the two other Raman-active modes (E_g at 643 cm^{-1} and T_{2g} at 525 cm^{-1}, to be denoted as v_1 and v_5, respectively) are about an order of magnitude weaker. In this paper we therefore consider only the effect of the symmetric stretch mode, in which S-F bond length R changes with time during SF_6 vibration. To simulate the effect of the Raman pump pulse on the molecule, we follow Refs. [40,41]. Briefly, when a molecule is exposed to a Raman pump pulse, the nuclear wave function $\chi(q,t)$ satisfies the time-dependent Schrödinger equation

$$i \frac{\partial \chi(q,t)}{\partial t} = \left(-\frac{1}{2\mu} \frac{\partial^2}{\partial q^2} + U(q) - \frac{1}{2} \sum_{i,j} \alpha_{ij}(q) E_i(t) E_j(t) \right) \times \chi(q,t). \quad (1)$$

Here, q is the normal coordinate for the symmetric stretch mode, μ is the reduced mass, $U(q)$ is the potential-energy surface, α is the polarizability tensor, and E_i is the component of the electric field of the laser pulse along the i axis. The polarizability tensor is calculated from the Gaussian 03 code [42], within the Hartree–Fock approximation with an augmented correlation-consistent polarized valence triple-zeta (aug-cc-pVTZ) basis set. We have also checked that density functional methods give somewhat different values for polarizability (up to about 20%). Nevertheless, $\partial \alpha_{ij}/\partial q$ remains quite stable and the results for vibrational wave packet are quite similar. The potential energy is approximated by a harmonic oscillator, which should be adequate for small-amplitude vibration considered in this paper. A pump with intensity of 5×10^{13} W/cm^2, wavelength of 790 nm, and pulse duration of 13 fs is used. With such a pump, ionization is insignificant (ionization potential of SF_6 is 15.7 eV). We also expect that the molecule remains in the ground electronic state.

By solving Eq. (1) numerically, we found that the population in $v_1 = 0$ and 1 states are about 85% and 14%, respectively, quite comparable with Wagner *et al.* [39]. The calculated nuclear wave packet distributions at different time delays, before the pump, at the end of the pump, and 36 fs after the pump, are shown in Fig. 2. The peak position of the wave packet changes only slightly; less than about ± 0.1 a.u. from the equilibrium distance at $R = 2.9$ a.u. We will show below that this small-amplitude vibration can be "imaged" with our method. We remark that the vibrational period is about 43 fs, consistent with the known vibrational period for SF_6 symmetric stretch mode. Increasing the pump-pulse duration to about 30 fs does not change our results significantly.

B. Theoretical calculation of photoelectron signals

Photoionization from $S(2p)$ by a soft-x-ray probe pulse can be modeled by standard molecular photoionization theory. Briefly, the differential photoionization cross section for a transition from an initial state Ψ_i to a final state Ψ_k^- can be
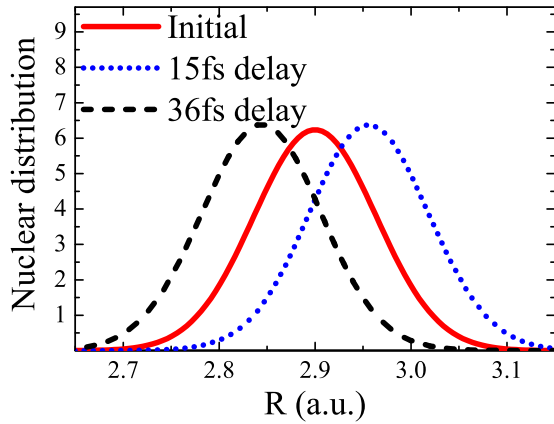
FIG. 2. Nuclear wave packet corresponding to symmetric stretch mode (ν_1) before the pump (solid curve), and 15 fs and 36 fs after the pump pulse, in dotted and dashed curve, respectively. For the pump-pulse parameters, see text.

written as follows:

$$\frac{d^2\sigma}{d\Omega_k d\Omega_n} = \frac{4\pi\omega k}{c}|\langle\Psi_i|\mathbf{r}\cdot\mathbf{n}|\Psi_k^-\rangle|^2, \tag{2}$$

where $\mathbf{n}$ is the direction of the pulse polarization, k is the momentum of the ejected photoelectron, $k^2/2 + I_p = \omega$ with I_p being the ionization potential, ω is the photon energy, and c is the speed of light. In this paper we use ePolyScat package [43,44] to compute Eq. (2). Note that we neglect spin-orbit coupling in our calculations. The initial molecular wave function is calculated by using the Gaussian 03 code [42] within the Hartree–Fock approximation with an augmented correlation-consistent polarized valence triple-zeta (aug-cc-pVTZ) basis set. At equilibrium the structure of SF_6 has O_h point group symmetry, with the S-F bond length of 1.536 Å.

We present in Fig. 3(a) the total (integrated) photoionization cross section (PICS) vs energy and S-F bond length from $2t_{1u}$ molecular orbital [to be referred to as $S(2p)$ in the following—see Fig. 1(a)] obtained with the ePolyScat package [43,44] with photon energy near 185–205 eV, slightly above the $S(2p)$ threshold. The shape resonance can be seen clearly in this range of nuclear vibration. To have a more quantitative idea, we show in Fig. 3(b) the PICS for a molecule at the equilibrium geometry. The PICS shows a strong shape resonance for a photoelectron near 13 eV. The position of this peak agrees well with experimental data [34] and has been identified as $4e_g$. The peak would be reduced when averaging over the ground-state nuclear distribution is taken into account, which brings the calculated PICS to a better agreement with Ferrett *et al.* [34]. We show in Fig. 3(b) the effect of this averaging for the vibrational ground state of the symmetric stretch mode (with $\nu_1 = 0$).

It is well known from molecular photoionization theory that shape resonance is typically quite sensitive to the surrounding atomic environment which influences the potential that the photoelectron experiences during its emission from an inner shell. This is confirmed by our calculated PICS for different photoelectron energies as a function of R, as shown in Fig. 3(a). At a more quantitative level, the PICS is also shown in Fig. 3(c) for a few energies as a function of S-F bond length. Indeed, the
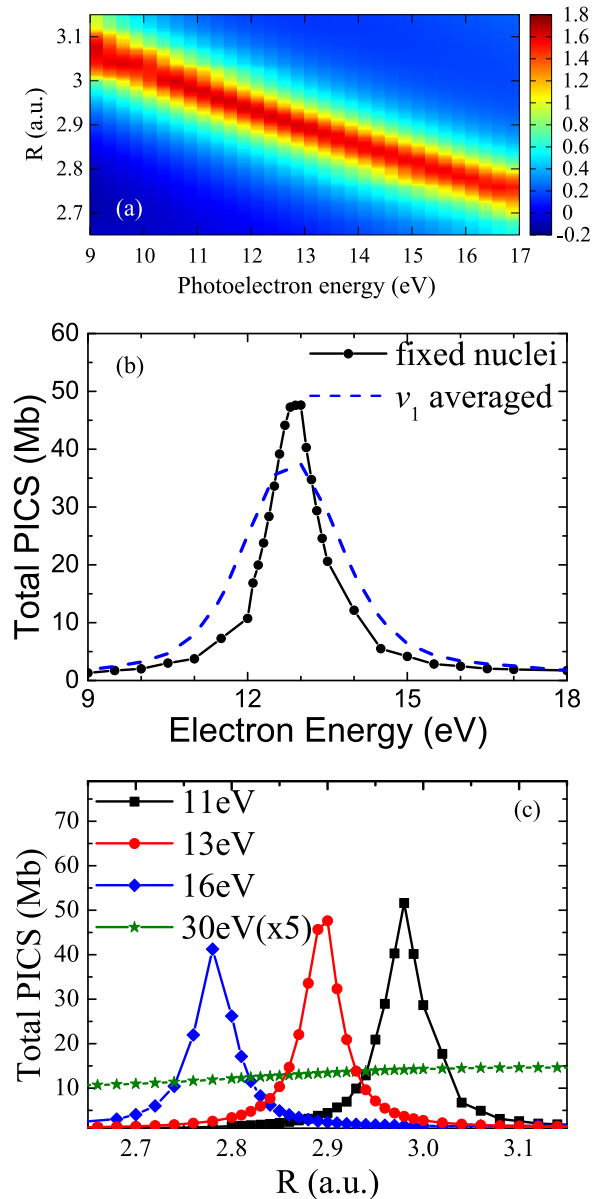
FIG. 3. (a) Total PICS (in logarithmic scale) vs photoelectron energy and S-F separation. (b) Total PICS vs photoelectron energy for SF_6 at equilibrium. Results after averaging over $\nu_1 = 0$ are shown as the dashed line. (c) Total PICS vs S-F internuclear distance R for a few photoelectron energies. The PICS at 30 eV has been multiplied by a factor of five.

PICS at photoelectron energy of 13 eV drops very fast within the range of the nuclear wave packet (see also Fig. 2). The peak of the PICS already moves beyond the range of nuclear wave packet for photoelectron only a few eV away from 13 eV. It is this sensitivity of PICS (and PAD, in general) that allows us to image small changes in nuclear wave packets during SF_6 vibration. At 30 eV, the shape resonance becomes very weak. Similar sensitivity for the PAD will be analyzed separately in Sec. III B. Since the molecular geometry changes only within a small parameter space near the equilibrium during its vibration after Raman excitation, it is more advantageous to probe it with photoelectrons with energies below about 30 eV

when the PICS experiences strong variation with respect to the S-F bond length.

Theoretically, total photoelectron signal ionized from $S(2p)$ at a particular energy E and probed at a time delay τ after the pump pulse can be modeled as

$$S(E,\tau) = \int \sigma(E,R)\rho(R,\tau)dR. \tag{3}$$

Here, $\rho(R,\tau)$ is the nuclear wave packet and $\sigma(E,R)$ is the total PICS at a fixed S-F bond length R. The above equation was written within the Chase adiabatic approximation [45] under the assumption that nuclei are frozen during the probe pulse. For a finite x-ray pulse with a duration of a few femtoseconds considered in this paper, a convolution over the photon spectral bandwidth is also carried out. A similar formula can also be applied for any given photoelectron emission direction.

A few remarks on the temporal scales involved are in order. Naturally we want to have a probe-pulse duration much shorter than the vibration period of the nuclear wave packet. In our case, we choose the probe pulse duration (full width at half maximum, or FWHM) of the order of about 1 fs, much smaller than the vibration period of the symmetric stretch mode (43 fs). With this choice, the nuclei will be frozen during the probe. The resonance width is about 1.5 eV for the whole range of S-F bond length during the nuclear vibration, see Fig. 3. Thus the resonance lifetime is estimated to be about 0.44 fs. The changes in nuclear positions during this decay time are negligible such that Eq. (3) is applicable.

III. RESULTS AND DISCUSSION

A. Analysis of photoelectron vs pump-probe delay time

Total PICS signal vs time delay is shown in Figs. 4(a)–4(d), for a few energies near the $4e_g$ shape resonance at 13 eV. Here the signals have been normalized to that from unexcited

ensemble (i.e., without the Raman pump pulse). For reference, we also show the averaged R (denoted as $\langle R \rangle$, right vertical axis) vs time delay. First, we focus on the case with a photoelectron of 13 eV, probed with a 1 fs pulse (FWHM), shown in Fig. 4(a). Interestingly, the normalized photoelectron signal shows a strong modulation with a period of about 21 fs, which is half of the period of the symmetric stretch mode. This can also be seen by comparing with $\langle R(\tau) \rangle$ curve. This behavior can be explained based on shape of the PICS at 13 eV and the wave packet shown in Figs. 3(b) and 2, respectively, in combination with Eq. (3). Indeed, during its vibration after the pump pulse, the wave packet probes both sides of the peak near $R = 2.9$ a.u. Note also that this peak is nearly symmetric with respect to $R = 2.9$ a.u. In particular, the wave packet passes through the peak of the PICS *twice* during a vibrational period. The peak-to-peak modulation amplitude is about 30%, which should be experimentally measurable. Changing the soft-x-ray-pulse duration to 2 fs does not change the results significantly; see the blue curve in Fig. 4(a).

In contrast, the case of 11 eV is totally different; see Fig. 4(b). Here, the modulation follows closely $\langle R(\tau) \rangle$ with the same period as the vibration period of symmetric stretch mode (43 fs). Again, this behavior reflects the dependence of the PICS vs R at this energy, which is probed by the nuclear wave packet. As can be seen from Figs. 2 and 3(c), the nuclear wave packet can mostly probe only one side of resonance shape (with $R < 3$ a.u.), where PICS increases monotonically with R. This correlation leads to in-phase modulation as compared to $\langle R(\tau) \rangle$. Also, since the probe spans only on one side of the shape resonance, the peak-to-peak modulation is much larger than that of the 13 eV case. At 16 eV, the photoelectron signal in Fig. 4(c) shows an out-of-phase modulation with respect to $\langle R(\tau) \rangle$. This is due to the fact that, in this case, the shape resonance is mostly probed with $R > 2.8$ a.u., for which the PICS decreases monotonically as a function of R. The modulation amplitude is also quite comparable to that of the 11 eV case, as can be expected. Note that, even at 30 eV, when the PICS does not show a clear peak within the range of accessible R, the modulation amplitude is still about 10%, see Fig. 4(d). Again, for this energy, the PICS slightly increases with R for the accessible range of the nuclear vibration, which results in the in-phase modulation as compared to $\langle R(\tau) \rangle$, although the modulation is much weaker than for the 11 eV case. Note that we did not perform averaging over the other vibration modes, which poses a great computational challenge at present.

We remark that probing the symmetric stretch mode in SF_6 can also be done, in principle, by measuring photoabsorption cross section with similar few-femtosecond soft-x-ray sources with photon energies near 200 eV. This is in the spirit of the near edge x-ray absorption fine structure (NEXAFS). Our method has access to more detailed information since, by detecting photoelectrons, different channels can be energetically separated.

FIG. 4. (a) Normalized total photoelectron signal at 13 eV with x-ray pulse of duration (FWHM) of 1 and 2 fs. Panels (b)–(d) are similar to panel (a) but for 11, 16, and 30 eV, respectively, for a 1 fs pulse. Averaged $\langle R(\tau) \rangle$ is also shown for comparison (dashed-lines, right vertical axes). In panel (c), the effect of random errors up to 10% is also shown (blue dots).

B. Analysis of photoelectron angular distribution

To be specific, we analyze here the behavior of the PAD at photoelectron energy of 13 eV. Let us first focus on the molecular-frame photoelectron angular distribution

(MFPAD). We show in Figs. 5(a)–5(c) the MFPAD for different S-F bond lengths of 2.8, 2.9, and 3.0 a.u., respectively. Here, the x-ray polarization is along z axis, which coincides with one of the S-F bonds. Clearly, the MFPAD changes quickly in both magnitude and shape with SF bond length near equilibrium. In particular, the lobe along the z axis appears to be quite pronounced for $R = 2.8$ and 2.9. a.u. but nearly disappears for $R = 3.0$ a.u. The lobe near $\{\theta,\phi\} = \{90°,45°\}$ and those obtained by rotation of 90°, 180°, and 270° about the z axis are much more pronounced at $R = 2.9$ a.u. than the other lobes, whereas the lobes are more comparable at the other values of R. We remark in passing that the analysis of the resonant state of the continuum electron has been reported in Refs. [35,38]. Although the MFPAD is not accessible experimentally for our target, we expect similar sensitivity near a shape resonance for other targets as well, for which the MFPAD or recoil-frame PAD (RFPAD) might be measurable. Furthermore, our results indicate that the sensitivity of the PAD with respect to the change in molecular geometry might survive in the laboratory-frame measurements, especially when target molecules are aligned.

By the same token we also expect that PAD vs delay time, especially from aligned molecules, provides much richer information than the PICS, which was discussed in the previous section. For the case of SF_6 (which is a spherical top molecule), the PAD dependence on photoelectron emission direction is quite weak; see Fig. 5(d) for a comparison between emission parallel and perpendicular to the x-ray polarization. It would be of interest in the future to explore the case of, say, symmetric top molecules which can be laser aligned [31,46].

C. Extraction of photoionization cross section

The results the the previous section prompt us to propose a simple method to extract PICS vs R from photoelectron signal vs time delay. In the absence of actual experimental data, in the following we will treat the photoelectron signals in Fig. 4 as "experimental" data $S^{\mathrm{expt}}(E,\tau)$. To simulate the effect of statistical error in experiments, we further add random errors up to about 10% to our data [see blue dots in Fig. 4(c) for the case of 16 eV]. We assume that the nuclear wave packet $\rho(R,\tau)$ is known from some theoretical calculation. For a fixed energy, in order to retrieve the PICS as a function of R, we model it by a Lorentzian form as follows:

$$\sigma^{\mathrm{theor}}(R) = B_0 + \frac{2A}{\pi}\frac{C}{(R - R_0)^2 + C^2}, \qquad (4)$$

with B_0, A, C, and R_0 as four parameters.

Under such assumptions, we can calculate theoretical photoelectron yield $S^{\mathrm{theor}}(E,\tau)$ using Eq. (3). By fitting theoretical results with "experimental" data $S^{\mathrm{expt}}(E,\tau)$, we identify the parameters for the best fit. In this work, we use the least-square fitting for each fixed energy as

$$\chi = \sum_{\tau_i} \left[\frac{S^{\mathrm{theor}}(E,\tau_i) - S^{\mathrm{expt}}(E,\tau_i)}{S^{\mathrm{expt}}(E,\tau_i)}\right]^2, \qquad (5)$$

such that the minimum in χ gives the best fit.

The results of this procedure are shown in Fig. 6 for different photoelectron energies. The retrieved PICS indeed
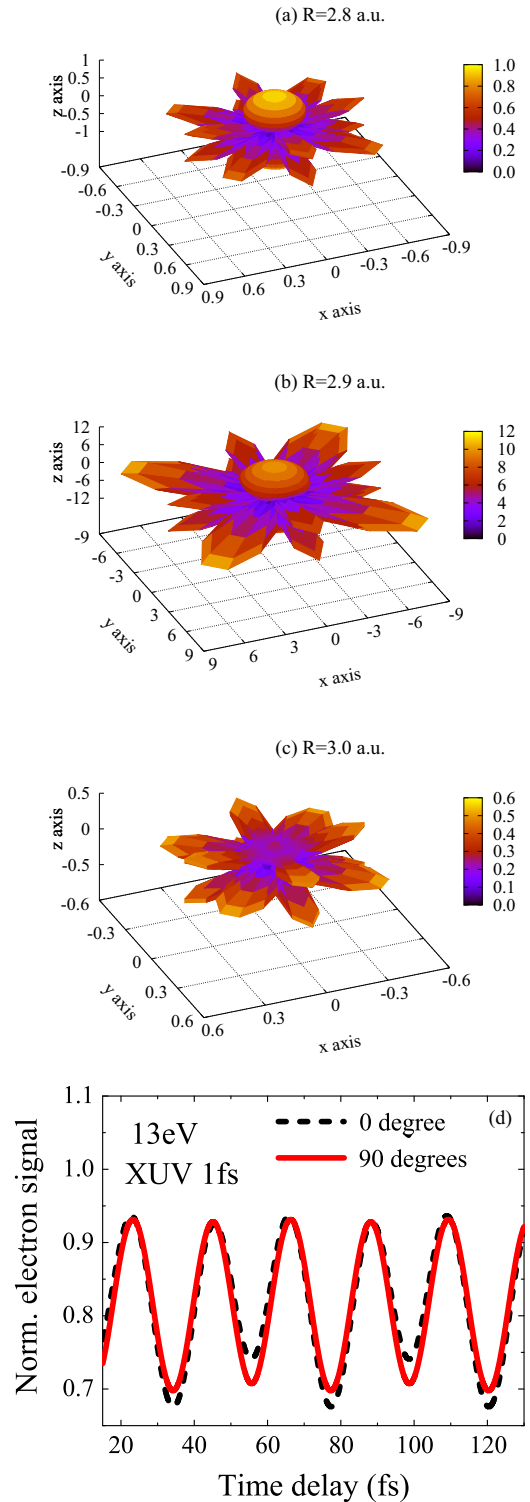
FIG. 5. (a)–(c) MFPAD of SF_6 (in units of Mb/steradian) with different S-F bond lengths of 2.8, 2.9, and 3.0 a.u., respectively. The sulfur atom is at the origin, while the fluorine atoms are located on the x, y, and z axes. The x-ray is polarized parallel to the z axis. The magnitude of MFPAD at each emission direction is given as the radial distance from the origin and is also color coded. (d) Photoelectron signals emitted along the parallel and perpendicular directions with respect to the x-ray polarization. The signals have been normalized to that of the unexcited ensemble. X-ray-pulse duration (FWHM) is 1 fs. The photoelectron kinetic energy is 13 eV in all panels.
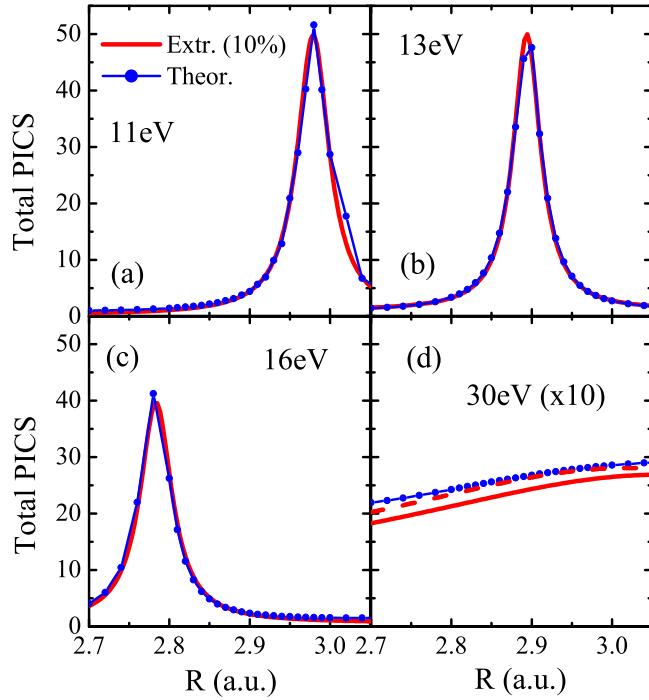
FIG. 6. Extracted total PICS from $S(2p)$ of SF_6 corresponding to photoelectron energy of (a) 11 eV, (b) 13 eV, (c) 16 eV, and (d) 30 eV. The "original" theoretical data obtained from ePolyScat are also shown. For the 30 eV case, the results with 5% random errors are also shown (dashed line). For each energy, the percent error is defined with respect to the largest signal in the case of 16 eV.

agree well with the ePolyScat results for all cases. Note that the PICS can only be retrieved for the range of R where the nuclear wave packet is non-negligible during the vibration. This results clearly indicate that PICS, and more generally PAD, at nonequilibrium geometries can be accessible from experimental measurements.

D. Extraction of nuclear wave packet

If the PAD can be calculated theoretically with sufficient accuracy and efficiency for a target with fixed geometry, the retrieval of bond lengths and bond angles from experimental data can be carried out. That has been demonstrated recently for static targets, for example, in Ref. [23]. In their retrieval procedure the multiple-scattering theory was used to fit to experimental PAD for relatively low photoelectron energy below about 200 eV. Similarly, Wang *et al.* [31] showed theoretically that bond lengths and bond angles can be retrieved by using relatively-high-energy PAD from laser-aligned molecules, with photoelectron holography theory. In those examples, the nuclei are assumed to be at fixed positions (i.e., without any distribution).

Here we show that we can extract the nuclear wave packet during its evolution in real time after the Raman excitation. Again, we treat results of Fig. 4 with the addition of random errors up to 10% as "experimental" data. We now further assume that PICS can be calculated theoretically with a sufficiently good precision for a fixed geometry near equilibrium. The unknown nuclear wave packet is modeled by
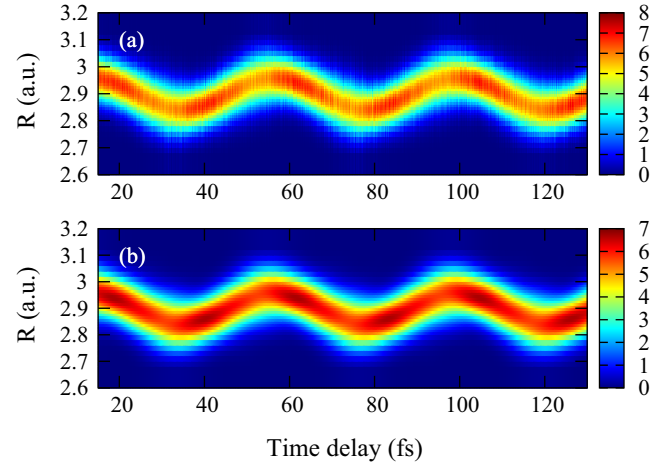
FIG. 7. (a) Extracted nuclear wave packet. (b) Nuclear wave packet obtained from numerical solution of the time-dependent Schrödinger equation.

a Gaussian form as

$$\rho(R) = A \exp\left[-\frac{(R - R_0)^2}{C^2}\right]. \quad (6)$$

In Eq. (6), parameters A, C, and R_0 vary as functions of time delay τ. We can then calculate the photoelectron signal by using Eq. (3) and compare with "experimental" signals to find the best fit. At each time delay τ, the least-square fitting is used as

$$\chi = \sum_{E_i} \left[\frac{S^{\text{theor}}(E_i, \tau) - S^{\text{expt}}(E_i, \tau)}{S^{\text{expt}}(E_i, \tau)}\right]^2. \quad (7)$$

The result of this procedure is shown in Fig. 7(a), which agrees well with the nuclear wave packet obtained from numerical solution of the time-dependent Schrödinger equation, shown in Fig. 7(b).

IV. SUMMARY AND OUTLOOK

In conclusion, we have shown, by using the example of vibrating SF_6 probed by a short x-ray pulse, that photoelectron signals contain sufficient information to allow us to extract target molecular structure and/or the dynamic changes in the nuclear wave packets in real time. Although we assumed that only a single vibration mode is available, inclusion of additional vibration modes should be straightforward. Our method utilizes the sensitivity of the photoelectron signals with respect to the changes in the surrounding atomic position relative to the inner-shell where the electron is emitted. As such, the method is more suitable for low-energy photoelectrons.

Our method should also be applicable for probing large-amplitude vibrations, which can be Raman excited in targets with relatively shallow potential-energy surfaces (PESs) near their equilibrium geometry (see, for example, Refs. [12,41]). To probe a broader range of R, one can increase the intensity of the pump laser. However, one cannot increase the laser intensity too much because it leads to excessive multiphoton ionization of the molecules. The emitted electron might potentially contaminate the photoelectron signals,

especially at low energies. To avoid this issue, one can use a pump-pump scheme with a optimized delay between the two pump pulses. Such a scheme has been proposed before; for example, in Refs. [47–49], where it is used to enhance molecular alignment and orientation. Furthermore, it should be possible to extend the method to the case when the target is prepared in electronically excited states, in particular dissociating or predissociating states, in which the nuclear wave packet experiences significant dynamical changes.

We remark that Wagner *et al.* [39] have shown that small-amplitude vibrations in SF_6 can be followed by HHG spectroscopy. In essence, photorecombination (time-reversed of photoionization) is embedded in HHG signals. Nevertheless, care must be taken to disentangle it from other steps in HHG [50].

While it is true that current attosecond sources are limited by the energy range and photon counts, we anticipate the situation to change in the near future thanks to the rapid progress in laser and XFEL technologies that we have witnessed recently [51–53]. Indeed, recent progress in HHG using mid-infrared driving lasers has pushed the photon energy up to a few-keV region [54], while attosecond pulses in the soft x-ray up to 0.5 keV have been reported using a transient phase-matching

mechanism [55]. Recent development in laser sources with high repetition rates of hundreds of kHz [56,57] as well as improved phase matching with waveguide setup will likely increase the HHG yields further in the near future. The x-ray pulses with duration down to a few femtoseconds are also becoming available at XFEL facilities such as LCLS (at Stanford) [3], SACLA (Japan) [4,5], and FLASH (Hamburg), depending on the photon energy range. The Extreme Light Infrastructure Attosecond Light Pulse Source (ELI-ALPS) in Szeged, Hungary, is currently under construction, with the promise of providing an ultrashort light source with a broad range of energy (see, for example, Ref. [58]).

[1] T. Brabec and F. Krausz, Rev. Mod. Phys. **72**, 545 (2000).

[2] H. N. Chapman, A. Barty, M. J. Bogan, S. Boutet, M. Frank, S. P. Hau-Riege, S. Marchesini, B. W. Woods, S. Bajt, W. H. Benner, R. A. London, E. Plönjes, M. Kuhlmann, R. Treusch, S. Düsterer, T. Tschentscher, J. R. Schneider, E. Spiller, T. Möller, C. Bostedt, M. Hoener, D. A. Shapiro, K. O. Hodgson, D. van der Spoel, F. Burmeister, M. Bergh, C. Caleman, G. Huldt, M. M. Seibert, F. R. N. C. Maia, R. W. Lee, A. Szöke, N. Timneanu, and J. Hajdu, Nat. Phys. **2**, 839 (2006).

[3] P. Emma, R. Akre, J. Arthur, R. Bionta, C. Bostedt, J. Bozek, A. Brachmann, P. Bucksbaum, R. Coffee, F.-J. Decker, Y. Ding, D. Dowell, S. Edstrom, A. Fisher, J. Frisch, S. Gilevich, J. Hastings, G. Hays, P. Hering, Z. Huang, R. Iverson, H. Loos, M. Messerschmidt, A. Miahnahri, S. Moeller, H.-D. Nuhn, G. Pile, D. Ratner, J. Rzepiela, D. Schultz, T. Smith, P. Stefan, H. Tompkins, J. Turner, J. Welch, W. White, J. Wu, G. Yocky, and J. Galayda, Nat. Photonics **4**, 641 (2010).

[4] D. Pile, Nat. Photonics **5**, 456 (2011).

[5] T. Ishikawa, H. Aoyagi, T. Asaka, Y. Asano, N. Azumi, T. Bizen, H. Ego, K. Fukami, T. Fukui, Y. Furukawa, S. Goto, H. Hanaki, T. Hara, T. Hasegawa, T. Hatsui, A. Higashiya, T. Hirono, N. Hosoda, M. Ishii, T. Inagaki, Y. Inubushi, T. Itoga, Y. Joti, M. Kago, T. Kameshima, H. Kimura, Y. Kirihara, A. Kiyomichi, T. Kobayashi, C. Kondo, T. Kudo, H. Maesaka, X. M. Maréchal, T. Masuda, S. Matsubara, T. Matsumoto, T. Matsushita, S. Matsui, M. Nagasono, N. Nariyama, H. Ohashi, T. Ohata, T. Ohshima, S. Ono, Y. Otake, C. Saji, T. Sakurai, T. Sato, K. Sawada, T. Seike, K. Shirasawa, T. Sugimoto, S. Suzuki, S. Takahashi, H. Takebe, K. Takeshita, K. Tamasaku, H. Tanaka, R. Tanaka, T. Tanaka, T. Togashi, K. Togawa, A. Tokuhisa, H. Tomizawa, K. Tono, S. Wu,

M. Yabashi, M. Yamaga, A. Yamashita, K. Yanagida, C. Zhang, T. Shintake, H. Kitamura, and N. Kumagai, Nat. Photonics **6**, 540 (2012).

[6] M. P. Minitti, J. M. Budarz, A. Kirrander, J. S. Robinson, D. Ratner, T. J. Lane, D. Zhu, J. M. Glownia, M. Kozina, H. T. Lemke, M. Sikorski, Y. Feng, S. Nelson, K. Saita, B. Stankus, T. Northey, J. B. Hastings, and P. M. Weber, Phys. Rev. Lett. **114**, 255501 (2015).

[7] A. H. Zewail, Annu. Rev. Phys. Chem. **57**, 65 (2006).

[8] M. Lein, J. Phys. B: At., Mol. Opt. Phys. **40**, R135 (2007).

[9] T. Morishita, A.-T. Le, Z. Chen, and C. D. Lin, Phys. Rev. Lett. **100**, 013903 (2008).

[10] A.-T. Le, R. R. Lucchese, M. T. Lee, and C. D. Lin, Phys. Rev. Lett. **102**, 203001 (2009).

[11] O. Smirnova, Y. Mairesse, S. Patchkovskii, N. Dudovich, D. Villeneuve, P. Corkum, and M. Y. Ivanov, Nature (London) **460**, 972 (2009).

[12] W. Li, X. Zhou, R. Lock, S. Patchkovskii, A. Stolow, H. C. Kapteyn, and M. M. Murnane, Science **322**, 1207 (2008).

[13] C. D. Lin, A.-T. Le, Z. Chen, T. Morishita, and R. Lucchese, J. Phys. B: At., Mol. Opt. Phys. **43**, 122001 (2010).

[14] M. Okunishi, T. Morishita, G. Prümper, K. Shimada, C. D. Lin, S. Watanabe, and K. Ueda, Phys. Rev. Lett. **100**, 143001 (2008).

[15] D. Ray, B. Ulrich, I. Bocharova, C. Maharjan, P. Ranitovic, B. Gramkow, M. Magrakvelidze, S. De, I. V. Litvinyuk, A. T. Le, T. Morishita, C. D. Lin, G. G. Paulus, and C. L. Cocke, Phys. Rev. Lett. **100**, 143002 (2008).

[16] M. Meckel, D. Comtois, D. Zeidler, A. Staudte, D. Pavičić, H. C. Bandulet, H. Pépin, J. C. Kieffer, R. Dörner, D. M. Villeneuve, and P. B. Corkum, Science **320**, 1478 (2008).

[17] C. I. Blaga, J. Xu, A. D. DiChiara, E. Sistrunk, K. Zhang, P. Agostini, T. A. Miller, L. F. DiMauro, and C. D. Lin, Nature (London) **483**, 194 (2012).

[18] M. Pullen, B. Wolter, A. T. Le, M. Baudisch, M. Hemmer, A. Senftleben, C. D. Schröter, J. Ullrich, R. Moshammer, C. D. Lin, and J. Biegert, Nat. Commun. **6**, 7262 (2015).

[19] C. Z. Bisgaard, O. J. Clarkin, G. Wu, A. M. D. Lee, O. Geßner, C. C. Hayden, and A. Stolow, Science **323**, 1464 (2009).

[20] P. Hockett, C. Z. Bisgaard, O. J. Clarkin, and A. Stolow, Nat. Phys. **7**, 612 (2011).

[21] F. Krasniqi, B. Najjari, L. Strüder, D. Rolles, A. Voitkiv, and J. Ullrich, Phys. Rev. A **81**, 033411 (2010).

[22] R. Boll, D. Anielski, C. Bostedt, J. D. Bozek, L. Christensen, R. Coffee, S. De, P. Decleva, S. W. Epp, B. Erk, L. Foucar, F. Krasniqi, J. Küpper, A. Rouzée, B. Rudek, A. Rudenko, S. Schorb, H. Stapelfeldt, M. Stener, S. Stern, S. Techert, S. Trippel, M. J. J. Vrakking, J. Ullrich, and D. Rolles, Phys. Rev. A **88**, 061402(R) (2013).

[23] M. Kazama, T. Fujikawa, N. Kishimoto, T. Mizuno, J. I. Adachi, and A. Yagishita, Phys. Rev. A **87**, 063417 (2013).

[24] K. Ueda, C. Miron, E. Plésiat, L. Argenti, M. Patanen, K. Kooser, D. Ayuso, S. Mondal, M. Kimura, K. Sakai, O. Travnikova, A. Palacios, P. Decleva, E. Kukk, and F. Martín, J. Chem. Phys. **139**, 124306 (2013).

[25] E. Plésiat, L. Argenti, E. Kukk, C. Miron, K. Ueda, P. Decleva, and F. Martín, Phys. Rev. A **85**, 023409 (2012).

[26] J. B. Williams, C. S. Trevisan, M. S. Schöffler, T. Jahnke, I. Bocharova, H. Kim, B. Ulrich, R. Wallauer, F. Sturm, T. N. Rescigno, A. Belkacem, R. Dörner, T. Weber, C. W. McCurdy, and A. L. Landers, J. Phys. B: At., Mol. Opt. Phys. **45**, 194003 (2012).

[27] C. S. Trevisan, C. W. McCurdy, and T. N. Rescigno, J. Phys. B: At., Mol. Opt. Phys. **45**, 194002 (2012).

[28] B. Zimmermann, D. Rolles, B. Langer, R. Hentges, M. Braune, S. Cvejanovic, O. Geßner, F. Heiser, S. Korica, T. Lischke, A. Reinköster, J. Viefhaus, R. Dörner, V. McKoy, and U. Becker, Nat. Phys. **4**, 649 (2008).

[29] J. Söderström, N. Mårtensson, O. Travnikova, M. Patanen, C. Miron, L. J. Sæthre, K. J. Børve, J. J. Rehr, J. J. Kas, F. D. Vila, T. D. Thomas, and S. Svensson, Phys. Rev. Lett. **108**, 193005 (2012).

[30] K. Nakajima, T. Teramoto, H. Akagi, T. Fujikawa, T. Majima, S. Minemoto, K. Ogawa, H. Sakai, T. Togashi, K. Tono, S. Tsuru, K. Wada, M. Yabashi, and A. Yagishita, Sci. Rep. **5**, 14065 (2015).

[31] X. Wang, A.-T. Le, C. Yu, R. R. Lucchese, and C. D. Lin, Sci. Rep. **6**, 23655 (2016).

[32] R. K. Kushawaha, M. Patanen, R. Guillemin, L. Journel, C. Miron, M. Simon, M. N. Piancastelli, C. Skates, and P. Decleva, Proc. Natl. Acad. Sci. USA **110**, 15201 (2013).

[33] R. R. Lucchese and F. A. Gianturco, Int. Rev. Phys. Chem. **15**, 429 (1996).

[34] T. A. Ferrett, D. W. Lindle, P. A. Heimann, M. N. Piancastelli, P. H. Kobrin, H. G. Kerkhoff, U. Becker, W. D. Brewer, and D. A. Shirley, J. Chem. Phys. **89**, 4726 (1988).

[35] M. Stener, P. Bolognesi, M. Coreno, P. OKeeffe, V. Feyer, G. Fronzoni, P. Decleva, L. Avaldi, and A. Kivimaki, J. Chem. Phys. **134**, 174311 (2011).

[36] W. Jolly, K. Bomben, and C. Eyermann, At. Data Nucl. Data Tables **31**, 433 (1984).

[37] D. Holland, M. MacDonald, P. Baltzer, L. Karlsson, M. Lundqvist, B. Wannberg, and W. von Niessen, Chem. Phys. **192**, 333 (1995).

[38] J. Jose and R. Lucchese, Chem. Phys. **447**, 64 (2015).

[39] N. L. Wagner, A. Wüest, I. P. Christov, T. Popmintchev, X. Zhou, M. M. Murnane, and H. C. Kapteyn, Proc. Natl. Acad. Sci. USA **103**, 13279 (2006).

[40] Z. B. Walters, S. Tonzani, and C. H. Greene, J. Phys. B: At., Mol. Opt. Phys. **40**, F277 (2007).

[41] A.-T. Le, T. Morishita, R. R. Lucchese, and C. D. Lin, Phys. Rev. Lett. **109**, 203004 (2012).

[42] M. J. Frisch, G. W. Trucks, H. B. Schlegel, G. E. Scuseria, M. A. Robb, J. R. Cheeseman, J. A. Montgomery, Jr., T. Vreven, K. N. Kudin, J. C. Burant, J. M. Millam, S. S. Iyengar, J. Tomasi, V. Barone, B. Mennucci, M. Cossi, G. Scalmani, N. Rega, G. A. Petersson, H. Nakatsuji, M. Hada, M. Ehara, K. Toyota, R. Fukuda, J. Hasegawa, M. Ishida, T. Nakajima, Y. Honda, O. Kitao, H. Nakai, M. Klene, X. Li, J. E. Knox, H. P. Hratchian, J. B. Cross, V. Bakken, C. Adamo, J. Jaramillo, R. Gomperts, R. E. Stratmann, O. Yazyev, A. J. Austin, R. Cammi, C. Pomelli, J. W. Ochterski, P. Y. Ayala, K. Morokuma, G. A. Voth, P. Salvador, J. J. Dannenberg, V. G. Zakrzewski, S. Dapprich, A. D. Daniels, M. C. Strain, O. Farkas, D. K. Malick, A. D. Rabuck, K. Raghavachari, J. B. Foresman, J. V. Ortiz, Q. Cui, A. G. Baboul, S. Clifford, J. Cioslowski, B. B. Stefanov, G. Liu, A. Liashenko, P. Piskorz, I. Komaromi, R. L. Martin, D. J. Fox, T. Keith, M. A. Al-Laham, C. Y. Peng, A. Nanayakkara, M. Challacombe, P. M. W. Gill, B. Johnson, W. Chen, M. W. Wong, C. Gonzalez, and J. A. Pople, *Gaussian 03, Revision C.02* (Gaussian, Inc., Wallingford, 2004).

[43] F. A. Gianturco, R. R. Lucchese, and N. Sanna, J. Chem. Phys. **100**, 6464 (1994).

[44] A. P. P. Natalense and R. R. Lucchese, J. Chem. Phys. **111**, 5344 (1999).

[45] D. M. Chase, Phys. Rev. **104**, 838 (1956).

[46] H. Stapelfeldt and T. Seideman, Rev. Mod. Phys. **75**, 543 (2003).

[47] X. Ren, V. Makhija, A.-T. Le, J. Troß, S. Mondal, C. Jin, V. Kumarappan, and C. Trallero-Herrero, Phys. Rev. A **88**, 043421 (2013).

[48] X. Ren, V. Makhija, and V. Kumarappan, Phys. Rev. Lett. **112**, 173602 (2014).

[49] P. M. Kraus, D. Baykusheva, and H. J. Wörner, Phys. Rev. Lett. **113**, 023001 (2014).

[50] A.-T. Le, R. R. Lucchese, S. Tonzani, T. Morishita, and C. D. Lin, Phys. Rev. A **80**, 013401 (2009).

[51] D. Gauthier, P. R. Ribič, G. De Ninno, E. Allaria, P. Cinquegrana, M. B. Danailov, A. Demidovich, E. Ferrari, and L. Giannessi, Phys. Rev. Lett. **116**, 024801 (2016).

[52] F. Campi, H. Coudert-Alteirac, M. Miranda, L. Rading, B. Manschwetus, P. Rudawski, A. L'Huillier, and P. Johnsson, Rev. Sci. Instrum. **87**, 023106 (2016).

[53] Z. Chang, P. B. Corkum, and S. R. Leone, J. Opt. Soc. Am. B **33**, 1081 (2016).

[54] T. Popmintchev, M.-C. Chen, D. Popmintchev, P. Arpin, S. Brown, S. Ališauskas, G. Andriukaitis, T. Balciunas, O. D. Mücke, A. Pugzlys, A. Baltuška, B. Shim, S. E. Schrauth, A.

Gaeta, C. Hernández-García, L. Plaja, A. Becker, A. Jaron-Becker, M. M. Murnane, and H. C. Kapteyn, Science **336**, 1287 (2012).

[55] S. M. Teichmann, F. Silva, S. L. Cousin, M. Hemmer, and J. Biegert, Nat. Commun. **7**, 11493 (2016).

[56] A. Thai, M. Hemmer, P. K. Bates, O. Chalus, and J. Biegert, Opt. Lett. **36**, 3918 (2011).

[57] J. Rothhardt, S. Hädrich, Y. Shamir, M. Tschnernajew, R. Klas, A. Hoffmann, G. K. Tadesse, A. Klenke, T. Gottschall, T. Eidam, R. Boll, C. Bomme, H. Dachraoui, B. Erk, M. Di Fraia, D. A. Horke, T. Kierspel, T. Mullins, A. Przystawik, E. Savelyev, J. Wiese, T. Laarmann, J. Küpper, D. Rolles, J. Limpert, and A. Tünnermann, arXiv:1602.03703.

[58] http://www.eli-alps.hu/?q=en/02_Parameters.